

Magnetization-density distribution in the metallic ferromagnet SrRuO₃ determined by polarized neutron diffraction

S. Kunkemöller,¹ K. Jenni,¹ D. Gorkov,^{1,2,3} A. Stunault,⁴ S. Streltsov,^{5,6} and M. Braden^{1,*}

¹*II. Physikalisches Institut, Universität zu Köln, Zùlpicher Str. 77, D-50937 Köln, Germany*

²*Heinz Maier-Leibnitz Zentrum, Technische Universität München, D-85748 Garching, Germany*

³*Physik-Department, Technische Universität München, D-85748 Garching, Germany*

⁴*Institut Laue Langevin, 6 Rue Jules Horowitz BP 156, F-38042 Grenoble CEDEX 9, France*

⁵*Ural Federal University, 620002 Yekaterinburg, Russia*

⁶*M. N. Miheev Institute of Metal Physics, Russian Academy of Sciences, 620137 Yekaterinburg, Russia*

(Dated: February 2, 2022)

The magnetization-density distribution in the metallic ferromagnet SrRuO₃ was studied by means of polarized neutron diffraction. The analyzes by multipole refinements and by the maximum entropy method consistently reveal a strong polarization of all oxygen sites carrying 30% of the total magnetization. The spin-density distribution on the Ru site exhibits a nearly cubic shape in agreement with an almost equal occupation of t_{2g} orbitals and pd hybridization. The experimental analysis is well reproduced by density functional calculations. There is no qualitative change in the magnetization distribution between 2 and 200 K.

I. INTRODUCTION

SrRuO₃ is a material with fascinating properties^{1–3} and has a strong application potential as an electrode for functional perovskites. It is metallic and exhibits ferromagnetic ordering below the Curie temperature of $T_C=165$ K³. There is strong coupling between the magnetism and charge carriers as the resistivity sharply drops at the ferromagnetic ordering^{4,5}. At low temperature high-quality single crystals exhibit good conductivity but well above the ferromagnetic order the resistivity increases with temperature exceeding the Ioffe-Regel limit already at moderate temperatures⁴. Non-Fermi liquid behavior was reported at low temperature⁶ and an invar effect in the magnetic phase⁷. The material is furthermore known for its peculiar anomalous Hall effect, that changes sign slightly below T_C ^{3,8–12}. It is argued that the larger spin-orbit coupling in this 4d compound together with the exchange splitting of the electronic bands results in various Weyl points close to the Fermi level¹³, which are proposed to cause the anomalous Hall effect^{9,12}. More recently it was realized that Weyl physics may also influence the spin dynamics due to the intrinsic coupling of magnetization and current density. Neutron scattering studies of the gap of the spin-wave dispersion^{12,14} as well as of its stiffness¹⁴ reveal an anomalous softening in the ferromagnetic state that contrasts with the expected behavior of a simple ferromagnet. The temperature dependent occupation of the Weyl points leads to the peculiar temperature dependence of the anomalous Hall effect, and also causes softening of the magnon gap and stiffness^{9,12}.

Spin-orbit coupling has a strong impact in SrRuO₃ as can be learned from the sizeable anisotropy gap of about 1 meV^{14,16}. This strong anisotropy is also seen in the anisotropic magnetization curves^{15,17–19}. Due to two structural phase transitions at 975 and 800 K the crystal structure of initially cubic SrRuO₃ is heavily dis-

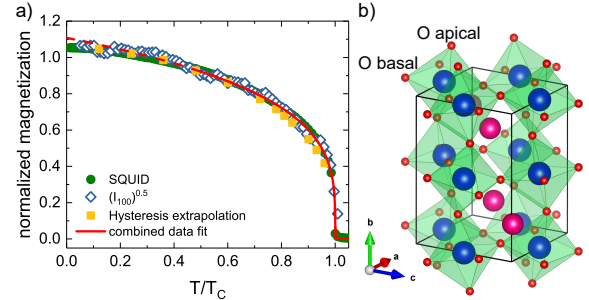


FIG. 1. (a) Temperature dependence of the magnetization compared with the square root of the extra scattering intensity at the $(100)_{cubic}$ Bragg reflection. For the magnetization we show the values obtained from extrapolating full hysteresis curves, data taken from Ref.¹⁴, and a temperature dependent measurement at $\mu_0 H=5$ mT parallel to a cubic $[110]$ direction. The three quantities perfectly scale with each other and are well described by a critical power law $m(T) \propto (1 - \frac{T}{T_C})^\beta$ with $\beta=0.27(2)$ fitted in the temperature range between $0.5T_C$ and T_C (red line). (b) Crystal structure of SrRuO₃ as determined by neutron diffraction at low temperature¹⁵.

torted at low temperatures with RuO₆ octahedra being rotated and tilted by about 9 degrees. The low-temperature space group is Pnma with lattice constants $a=5.53$, $b=7.85$, and $c=5.57$ Å^{1,20–23} and therefore single crystals of SrRuO₃ exhibit complex structural twinning with six domain orientations unless some detwinning procedure is applied. The easy axis of SrRuO₃ corresponds to the orthorhombic c direction, parallel to the longest edge of the RuO₆ octahedron¹⁵. Thus the magnetic moment points along the elongation of the RuO₆ octahedron in agreement with what one may expect from the spin-orbit coupling. Magnetization curves along the three orthorhombic directions indicate efficient anisotropies of the order of 10 T^{15,17–19} in perfect agreement with the microscopic anisotropy value of 1 meV¹⁴.

However, there are several conflicting reports due to the ability of SrRuO_3 to change its domain distribution as function of external magnetic field¹⁵. If the magnetic field is not applied along the easy axis parallel to the c direction in an untwinned single crystal the structural domains reorient. For magnetic field along a cubic $[110]$ direction, the structural domains with the orthorhombic c parallel to the field grow on the cost of the other domains. For field along cubic $[100]$, the domains with c direction at 45° to the field grow on the cost of those with c perpendicular to the field. This coupling of domains and magnetization can also explain some glassy processes^{24,25} that are not intrinsically magnetic but structural.

Recent density functional theory (DFT) calculations characterize SrRuO_3 as a moderately correlated electron system²⁶ in contrast to e.g. Ca_2RuO_4 being considered as a Mott insulator²⁷. SrRuO_3 seems not to be half metallic but the free charge carriers possess minority spin²⁸. The orbital moment is found by X-ray magnetic circular dichroism (XMCD) to be tiny, about two orders of magnitude smaller than the spin contribution^{29,30}; Agrestini et al. report $L_z/2S_z$ ratios of 0.01²⁹ and Okamoto et al. give an orbital moment of 0.04(4) Bohr magnetons³⁰. These very small orbital moments also agree with our DFT calculations, see below.

The perovskite SrRuO_3 furthermore is relevant for the understanding of the unconventional superconductor Sr_2RuO_4 because its ferromagnetism inspired the first proposals of p -wave triplet pairing in Sr_2RuO_4 ^{31,32}. Recent inelastic neutron scattering studies indeed find quasi-ferromagnetic fluctuations in Sr_2RuO_4 ³³, but they clearly differ from the magnon and paramagnon response³⁴ observed in SrRuO_3 ¹⁴. While the electronic structure is well studied and well understood to fine details in Sr_2RuO_4 , ARPES measurements of similar quality are lacking for SrRuO_3 .

Early DFT studies emphasized a large magnetization of the oxygen in SrRuO_3 , in total about one third of the magnetization would reside on the oxygen orbitals³⁵. Since oxygen orbitals can be polarized in a ferromagnetic but not in an antiferromagnetic arrangement of neighboring Ru spins, a q dependence of the electronic interaction parameter $I(q)$ was deduced³⁵; such interaction $I(q)$ is used in an RPA treatment³⁶ as well as in the BCS gap equation calculations^{33,37}. Experimental evidence for a large polarization of oxygen orbitals was indeed found in polarized neutron diffraction experiments on $\text{Ca}_{2-x}\text{Sr}_x\text{RuO}_4$, which exhibits a metamagnetic transition³⁸. The polarized measurement even allowed one to identify the Ru d_{xy} orbital as the one carrying the magnetization. More recently, the triple-layer member of the Ruddlesdon Popper series, $\text{Sr}_4\text{Ru}_3\text{O}_{10}$, was studied by polarized neutron diffraction³⁹, also revealing sizeable oxygen moments. But the complex crystal structure with many different oxygen sites limits the precision of the spin-density determination at various sites. Here we report on polarized neutron diffraction studies of the spin density in SrRuO_3 , which reveal that $\sim 30\%$ of the

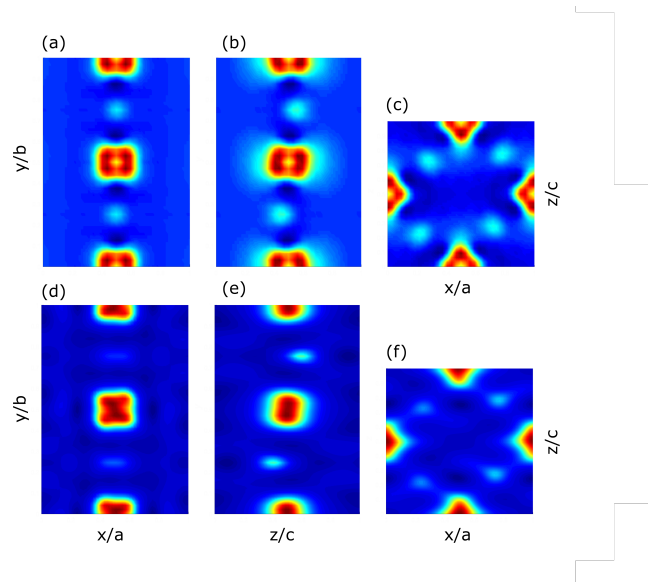


FIG. 2. Spin-density distribution maps in the $(x,y,0)$, $(0,y,z)$ and $(x,0,z)$ planes in the primitive cell perpendicular to the orthorhombic directions. All maps were obtained with the data set taken at 2K temperature and 9T magnetic field. The upper row (a-c) represents the results of the multipole refinement⁴⁶. The lower set of maps (d-f) represents the spin-density maps obtained with the maximum entropy algorithm.

magnetization are indeed carried by the oxygen orbitals. Thus pd hybridization cannot be ignored in ruthenates.

II. EXPERIMENTAL

Single crystals of SrRuO_3 were grown by the traveling floating-zone technique in a mirror furnace as described in¹⁹. The magnetization as function of temperature was determined in a commercial SQUID magnetometer (MPMS, Quantum Design). Unpolarized neutron diffraction experiments were performed at the KOMPASS instrument at the Maier Leibnitz Zentrum⁴⁰. A neutron beam with a wavelength of 4.00\AA was obtained with a highly oriented pyrolytic graphite monochromator and higher order contaminations were suppressed by a velocity selector. The instrument was operated in two-axis mode. The polarized neutron-diffraction measurements were performed at the Institut Laue Langevin using the spin polarized hot neutron diffractometer D3 in the high-field set up with a lifting-counter detector⁴¹. A 10 T cryomagnet was used and the Heusler monochromator produced a 95 % polarized neutron beam with a wavelength of 0.85\AA . Two Erbium filters were introduced to suppress higher order contaminations.

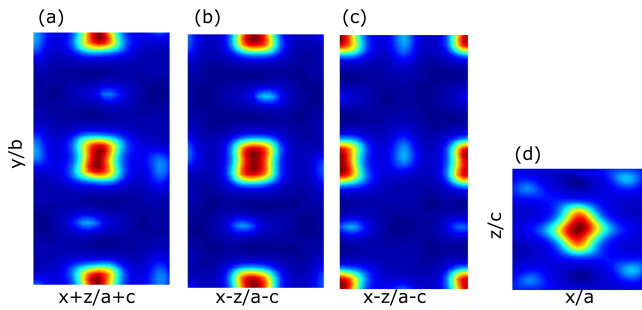


FIG. 3. Spin-density maps at 2 K as obtained by the maximum entropy algorithm. (a) shows a cut perpendicular to $[1\bar{1}0]$, which cuts the O octahedrons nearly at their corners. So the Ru position is in the middle of the picture. (b) shows a cut perpendicular to that shown in (a), again, the Ru position is placed at the middle of the picture. (c) shows a cut in the same direction like (b), but a basal O is placed in the middle of the picture. (d) shows a cut perpendicular to b at $y = 0$.

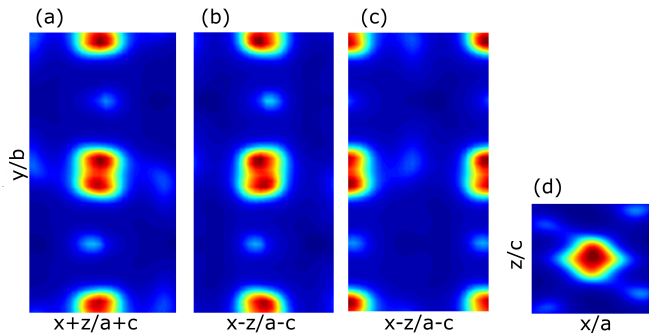


FIG. 4. Spin-density maps at 200 K as obtained by the maximum entropy algorithm. The same cuts as in Figure 3 are shown, but obtained with the data recorded at 200 K.

III. RESULTS AND DISCUSSION

A. Polarized and unpolarized neutron experiments

Figure 1 compares the temperature dependence of the magnetization in SrRuO_3 determined by the SQUID experiments with that obtained from the neutron diffraction study. In the unpolarized neutron diffraction experiment the magnetization is observed as an additional contribution to the $(100)_{\text{cubic}}$ Bragg reflection intensity, which is proportional to the square of the magnetization, the order parameter of the ferromagnetic transition. Indeed the magnetization and the square root of the additional (100) intensity scale very well with each other down to low temperature. For the magnetization we show the results obtained from extrapolating full hysteresis cycles, data taken from Ref.¹⁴, and a temperature dependent measurement with $\mu_0 H = 5$ mT parallel to the cubic $[110]$ direction (recorded after field cooling the sample in $\mu_0 H = 7$ T). The temperature dependence of the magnetization is well described by a critical power law

$m(T) \propto (1 - \frac{T}{T_c})^\beta$ with $\beta = 0.27(2)$ in agreement with previous powder analyzes $\beta = 0.25(1)^{12}$ and $\beta = 0.24(4)^{23}$. If only the more dense temperature dependent magnetization data is used to determine the critical exponent, we obtain $\beta = 0.267(4)$ with the data between $0.5T_c$ and T_c and $\beta = 0.262(6)$ with data between $0.9T_c$ and T_c . It is remarkable that the power law can very well describe the data down to half of the Curie temperature.

In the polarized neutron experiment we analyzed a nearly cube shaped piece of single crystalline SrRuO_3 ^{15,19} with a mass of 60 mg. The crystal edges corresponded to the orthorhombic directions, and the magnetic field was applied parallel to the c -direction. The sample was cooled down to 2 K in a field of 9 T. The magnetic field has two roles in the polarized neutron experiment, it aligns the spins of the sample and guides the neutron spins. The sample was mechanically detwinned before the neutron experiment yielding a strongly dominant, 85%, domain¹⁵. The magnetic field was applied parallel to the c direction of the main domain, which due to our previous neutron diffraction studies results in an almost complete monodomain state¹⁵. The absence of twinning is crucial for the precision of the spin-density analysis. A large set of 306 flipping ratios, i.e. ratios of the Bragg reflection intensities for neutron spin parallel and antiparallel to the external magnetic field, was measured at 2 K and after heating to 200 K another set of 177 flipping ratios was recorded. These sets contained 92 and 65 symmetrically inequivalent flipping ratios with weighted reliability factor values for equivalent reflections of 3.98 and 1.41%⁴¹.

The flipping ratio is given by the quotient of the squared sums and differences of nuclear and magnetic structure factors, and for a centrosymmetric system with magnetization perfectly aligned by the magnetic field it can be written as (without corrections for extinction and absorption)⁴²:

$$FR = \frac{F_N(hkl)^2 + 2sF_N(hkl)F_M(hkl) + sF_M(hkl)^2}{F_N(hkl)^2 - 2sF_N(hkl)F_M(hkl) + sF_M(hkl)^2},$$

where $F_N(hkl)$ is the nuclear structure factor, $F_M(hkl) = \frac{\gamma r_0}{2\mu_B} M(hkl)$ is the magnetic structure factor corresponding to the Fourier transform of the magnetization density, and $s = \sin^2(\alpha)$ with α the angle between the magnetic field and the scattering vector. The advantage of the flipping ratio method as compared to an unpolarized experiment stems from its enhanced sensitivity. If the magnetic intensity contribution amounts to one percent of the nuclear intensity in an unpolarized experiment, corresponding to $|F_M(hkl)| = 0.1|F_N(hkl)|$, and assuming $\sin(\alpha) = 1$, the flipping ratio already amounts to ~ 1.5 , which can be easily studied.

The flipping ratio data were used to determine the spin-density distribution by performing a least square refinement of magnetization models with the program FULLPROF^{43,44}, and by using the maximum entropy method (MEM) and routines implemented in the Cambridge Crystallography Subroutine Library (CCSL)⁴⁵.

TABLE I. Results of the refinements of the magnetization density models with the flipping ratios measured at 2 and 200 K. Moments at the Ru, apical and basal plane oxygens are given in Bohr magnetons, μ_B , the weighted reliability factor of the differences of the flipping ratios with one is given in per cent. Refinements are performed in space group Pnma with Ru at (0,0,0.5), O_{apic} at (-0.005,0.25,0.446) and O_{basal} at (0.278,0.029,0.722). The Sr ion sits at (0.022,0.25,-0.004) but does not carry magnetization.

2K	Ru_{tot}	Ru_{orb}	O_{apic}	O_{basal}	μ_{total}	R_{1-FR}
<i>mult</i>	0.85(5)	/	0.16(3)	0.17(2)	1.35(7)	16.1
<i>mono</i>	1.35(3)	0.36(8)	0.20(2)	0.20(2)	1.95(9)	25.2
<i>mono</i>	1.42(3)	/	0.20(2)	0.20(2)	2.00(9)	26.4
200K						
<i>mult</i>	0.29(2)	/	0.09(1)	0.06(1)	0.50(3)	4.2
<i>mono</i>	0.34(1)	0.16(3)	0.02(1)	0.026(6)	0.40(3)	8.3
<i>mono</i>	0.37(1)	/	0.01(1)	0.019(6)	0.42(2)	9.2

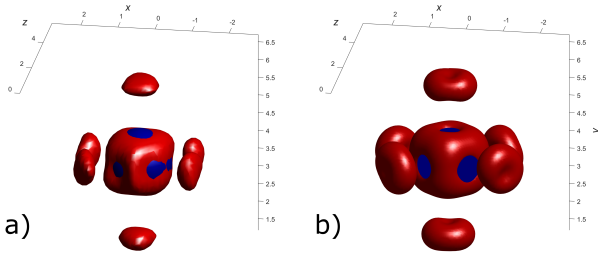


FIG. 5. (a) Three dimensional illustration of the magnetization-density distribution as determined with the maximum entropy algorithm; a full RuO_6 octahedron is shown in an isosurfaceplot corresponding to magnetization densities of $0.06 \mu_B/\text{\AA}^3$. (b) Magnetization-density distribution determined by spin polarized DFT calculations. This calculated spin density was determined by subtracting the majority and minority densities, which cancels out all contributions from fully occupied shells; the same isocontourplot as in (a) is shown. In (a) and (b) a blue sphere with radius 0.9\AA is drawn at the Ru position.

The MEM is a model free method to reconstruct the spin density. With the program FULLPROF two models for the spin density were refined. Firstly, a simple monopole model was refined with a maximum of two parameters per magnetic atom. In this dipole approximation one parameter corresponds to the total magnetic moment and the other one to the orbital contribution. Secondly, a multipole model was applied which allows one to describe an anisotropic shape of the spin density at the Ru site. The results of the monopole and multipole refinements are summarized in TABLE I and the comparison of calculated and observed flipping ratios is shown and discussed in the Appendix. The structural data were taken from structural analyzes performed by single-crystal neutron diffraction on comparable crystals, see Ref.¹⁵.

The focus of this study is set on the low-temperature

spin-density distribution. The dataset recorded at 2 K contains more reflections than the dataset recorded at 200 K. Additional reflections are either recorded at higher $\sin(\Theta)/\lambda$ or are superstructure reflections with respect to the high-temperature ideally cubic structure in space group $Fm\bar{3}m$. The latter contain no contribution of the Ru because the higher symmetry of the Ru site excludes a contribution at any superstructure reflection. These superstructure reflection data possess a strong weight in the refinement of the oxygen contribution to the spin density. The refinement of the monopole model with the data recorded at 2 K results in a total magnetic moment at the Ru site of $1.35(3) \mu_B$ and an orbital moment of $0.36(8) \mu_B$, see TABLE I. This orbital moment is much larger than values obtained by two soft XMCD studies^{29,30} and also our DFT calculations yield an orbital moment of only $0.007 \mu_B$. In the dipole approximation the entire, spin plus orbital, moment contributes to the magnetic formfactor through the spherical Bessel function of 0th order $j_0(Q)$ while only the orbital component also contributes through second order function $j_2(Q)$. There are no radial functions available for four-valent Ru so that the function for monovalent Ru was used in this and in other studies^{38,39}. The fitted large orbital moment seems to result from the inadequacy of the function and from the pronounced anisotropies. Furthermore the monopole fit with an orbital moment is only slightly better. In these monopole models both oxygen sites carry large moments, in total about one third of the entire magnetic moment. In the multipole refinement 14 parameters were used to describe the anisotropic spin density at the Ru site, while oxygen distributions were treated as monopoles. Again about one third of the total spin density is found at the oxygen positions. These large oxygen moments result from the large pd hopping and the near degeneracy of the Ru t_{2g} and O p states³⁵ and are also observed in layered ruthenate compounds either by neutron diffraction^{38,39} or in the magnetic excitations by inelastic neutron-scattering experiments⁴⁷. The fraction of oxygen moments to the total moment obtained with the monopole model, 31% in our $SrRuO_3$ experiment, can be directly compared with that observed for $Ca_{1.5}Sr_{0.5}RuO_4$, 31%³⁸, and that reported for $Sr_4Ru_3O_{10}$, 33%³⁹. The amount of transferred moment is thus very similar in these three metallic ruthenates underlining the universal character of the pd hybridization in ruthenates.

Addressing the anisotropic spin-density distribution demands the fit with a multipole model, which results in significantly smaller reliability values, R_{1-FR} , compared to the fit with the monopole model, see Table I and the Appendix. In Fig. 2 cuts through the spin-density distribution parallel to the orthorhombic axes can be seen. The spin density around the Ru position is clearly anisotropic. The magnetic moments on the O sites amount to $0.16(3)$ and $0.17(2) \mu_B$ for the apical and basal O, respectively, again about one third of the magnetization is carried by the oxygen orbitals.

Detailed plots of the spin density distribution can be obtained by an image reconstruction using the MEM⁴⁵. The spin density is discretized into 125000 pixels, 50 in each direction, and the reconstruction algorithm was used with a conventional flat density as start map, which tends to suppress artificial spin-density peaks. From this spin-density reconstruction the total magnetic moments can be obtained by numerical integration. The radius for the Ru position is chosen to be 1.2 Å and to 0.9 Å for the O positions. This leads to magnetic moments of 0.91 μ_B at the Ru site, of 0.07 μ_B at the apical O site and of 0.12 μ_B at the basal O site. The smaller moments at the oxygen sites result from the flat start map, that acts against local moments. The study on $\text{Ca}_{2-x}\text{Sr}_x\text{RuO}_4$ in Ref.³⁸ also found smaller magnetic moments with the MEM because of the negative bias against any local magnetic spin density. Keeping this tendency in mind, the observation of oxygen moments in the MEM reconstruction unambiguously confirms the sizeable magnetization carried by the oxygen orbitals. Besides the underestimation of the oxygen moments, there is an excellent agreement between the multipole refinements and the MEM reconstruction, see Fig. 2. In particular both methods also agree about the anisotropy of the spin-density distribution at the Ru site. Instead of a simple sphere we find a cube shaped distribution. In Figure 3 we show similar MEM maps along the orthorhombic diagonals, which are nearly parallel to the Ru-O bonds. Therefore, the oxygen moments become better visible in these maps. The comparison of these spin-density maps at 2K and 9T, see Fig. 3, with those at the same field and 200K, Fig. 4, indicates no qualitative differences besides the overall reduction of magnetic moments. This excludes an essential change in the character of the magnetization to occur between 200 and 2K. Therefore, the invar effect cannot be explained by a change in the local magnetization associated with changing orbital occupation. In Fig. 5, we present a three-dimensional plot of the MEM spin-density distribution for a single RuO_6 octahedron in form of an isocontourplot for a magnetization-density value of $0.06\mu_B/\text{\AA}^3$ at 2K and 9T. One recognizes the cube shape of the Ru spin density with the cube faces pointing perpendicular to the Ru-O bonds, while the spin density at the oxygen exhibits a disc shape with the discs being perpendicular to the bonds. All these features perfectly agree with our DFT calculations.

B. Spin-polarized DFT calculations

We have performed spin-polarized DFT calculations to construct the theoretical spin-density distribution, which is also visualized in figure 5. We used Perdew-Burke-Ernzerhof⁴⁸ version of the exchange-correlation potential and utilized pseudo-potential method (as realized in the VASP code⁴⁹). The mesh in k -space was chosen to be $6 \times 6 \times 4$. The plane wave cutoff energy was set to 600 eV. The crystal structure corresponding to T=10

K was taken from Ref.¹⁵, but ionic positions were relaxed until total energy change between ionic iterations exceeded 10^{-5} eV/u.c. (unit cell consists of 4 formula units). The magnetic moments on the Ru and O ions were found to be 1.34 μ_B and 0.13-0.16 μ_B respectively (they were calculated by integration of the spin density in the atomic spheres with radii 1.25 and 0.73 Å³), which perfectly agrees with the experiment. Thus also in the DFT calculations about one third of the magnetization resides on the oxygen orbitals. The calculated magnetization density is compared to the one determined by the MEM algorithm in figure 5. There is excellent agreement with the experimental density concerning the strong polarization of the oxygen sites and the peculiar anisotropy of the distribution at the Ru site, see Fig. 5. The Ru anisotropy can be attributed to the nearly equal occupation of the t_{2g} orbitals carrying the main part of the magnetization, while e_g orbitals are empty. In addition there is hybridization between the t_{2g} and the oxygen p orbitals perpendicular to the bond, which perfectly explains the cubic faces of the Ru spin density as well as the disc-shaped spin density at the O positions are both perpendicular to the bonds. E.g. for a Ru-O bond along the x direction the d_{xy} and d_{xz} may form π bonds with oxygen p_y and p_z orbitals, respectively, but hybridization of the p_x orbital is impossible for this bond.

IV. CONCLUSIONS

In conclusion we have studied the spin-density distribution in the metallic ferromagnetic SrRuO_3 by the flipping ratio method using polarized neutrons. The studied single crystal was first mechanically detwinned and the application of the magnetic field along the orthorhombic easy axis of the main domain results in an almost complete monodomain crystal. Due to the monodomain sample, high-quality data were obtained that can be easily analyzed in the orthorhombic structure yielding a high precision for the spin-density distribution. We may fully confirm the strong magnetic polarization of the oxygen orbitals that was deduced from early DFT calculations. Indeed about one third of the total magnetization is carried by the oxygen orbitals. Furthermore, the spin-density maps exhibit pronounced anisotropies at the Ru and oxygen sites that agree with the bonding and hybridization of the Ru $t_{2g}d$ and oxygen p orbitals. The experimental magnetization densities including this peculiar anisotropy agrees perfectly with the calculated one. The pd hybridization is an essential effect in all ruthenates and even stronger effects can be expected for 5d materials. Neglecting this transfer of magnetization will result in rather incorrect determination of magnetic moments for ferromagnetic as well as for antiferromagnetic ruthenates. The absence of a qualitative temperature dependence of the anisotropic magnetization density indicates that the orbital occupation in SrRuO_3 does not essentially change with temperature.

ACKNOWLEDGMENTS

This work was funded by the Deutsche Forschungsgemeinschaft (DFG, German Research Foundation) - Project number 277146847 - CRC 1238, projects A02 and B04. S.V.S thanks the Russian Ministry of Science and High Education, which supported the research through the program AAAA-A18-118020190095-4 (topic “Quantum”) and contract 02.A03.21.0006. We acknowledge stimulating discussions with T. Lorenz and D. Khomskii.

Appendix: Comparison of observed and calculated flipping ratios

The quality of the data and the refinements can be accessed by comparing the observed flipping ratios to those calculated with monopole and multipole models at the temperatures of 2 and 200 K, see Fig. 6. For both temperatures there is a clear improvement when passing from the monopole to the multipole models. While the 200 K data set can be very well described yielding a low reliability factor for the flipping ratios subtracted by one, this R_{1-FR} value remains larger, 16% , for the more complete 2 K data set even for the multipole model. One difference results from the larger number of superstruc-

ture reflections that were recorded at low temperature, and that exhibit smaller flipping ratios due to the absence of the Ru contributions. However, this cannot fully account for the larger R_{1-FR} value at 2 K. In the multipole model we assume monopole distributions at the two oxygen sites, which is inadequate in view of the maximum entropy and the DFT analysis. Refining also the multipole distributions for the two oxygen position induces 12 more parameters, which significantly limits the precision of all parameters but reduces the R value to 12.7% . Close inspection of the calculated and observed flipping ratios, see Fig. 6 (a,b), indicates that some stronger flipping ratios deviate more than their errors but that the majority of this data set is well described in the multipole model. In particular the (-141) reflection cannot be correctly described. This problem seems to arise from extinction, which becomes very anisotropic in the detwinned crystal¹⁵. For this particular reflection extinction can suffer from nearly perfect blocks being aligned parallel to the beam. Excluding this single reflection from in total 92 (inequivalent) reflections analyzed yields $R_{1-FR}=11.7\%$ for the model with only Ru described by a multipole, and $R_{1-FR}=7.0\%$ for the complete multipole model. In the text we discuss the Ru multipole refinement with the full data set, because there are no significant changes in the two refinements with only Ru multipole distributions. Note that extinction is better corrected in the MEM procedure.

-
- * e-mail: braden@ph2.uni-koeln.de
- ¹ J. J. Randall and R. Ward, *J. Am. Chem. Soc.* **81**, 2629 (1959).
 - ² A. Callaghan, C. W. Moeller, and R. Ward, *Inorg. Chem.* **5**, 1572 (1966).
 - ³ G. Koster, L. Klein, W. Siemons, G. Rijnders, J. S. Dodge, C.-B. Eom, D. H. A. Blank, and M. R. Beasley, *Rev. Mod. Phys.* **84**, 253 (2012).
 - ⁴ P. B. Allen, H. Berger, O. Chauvet, L. Forro, T. Jarlborg, A. Junod, B. Revaz, and G. Santi, *Physical Review B* **53**, 4393 (1996).
 - ⁵ L. Klein, J. S. Dodge, C. H. Ahn, G. J. Snyder, T. H. Geballe, M. R. Beasley, and A. Kapitulnik, *Phys. Rev. Lett.* **77**, 2774 (1996).
 - ⁶ P. Kostic, Y. Okada, N. C. Collins, Z. Schlesinger, J. W. Reiner, L. Klein, A. Kapitulnik, T. H. Geballe, and M. R. Beasley, *Phys. Rev. Lett.* **81**, 2498 (1998).
 - ⁷ T. Kiyama, K. Yoshimura, K. Kosuge, Y. Ikeda, and Y. Bando, *Phys. Rev. B* **54**, R756 (1996).
 - ⁸ M. Izumi, K. Nakazawa, Y. Bando, Y. Yoneda, and H. Terachi, *Journal of the Physical Society of Japan* **66**, 3893 (1997), <http://dx.doi.org/10.1143/JPSJ.66.3893>.
 - ⁹ Z. Fang, N. Nagaosa, K. S. Takahashi, A. Asamitsu, R. Mathieu, T. Ogasawara, H. Yamada, M. Kawasaki, Y. Tokura, and K. Terakura, *Science* **302**, 92 (2003), <http://www.sciencemag.org/content/302/5642/92.full.pdf>.
 - ¹⁰ Y. Kats, I. Genish, L. Klein, J. W. Reiner, and M. R. Beasley, *Phys. Rev. B* **70**, 180407 (2004).
 - ¹¹ N. Haham, Y. Shperber, M. Schultz, N. Naftalis, E. Shimshoni, J. W. Reiner, and L. Klein, *Phys. Rev. B* **84**, 174439 (2011).
 - ¹² S. Itoh, Y. Endoh, T. Yokoo, S. Ibuka, J.-G. Park, Y. Kaneko, K. S. Takahashi, Y. Tokura, and N. Nagaosa, *Nature Communications* **7**, 11788 (2016).
 - ¹³ Y. Chen, D. L. Bergman, and A. A. Burkov, *Phys. Rev. B* **88**, 125110 (2013).
 - ¹⁴ K. Jenni, S. Kunkemöller, D. Brünig, T. Lorenz, Y. Sidis, A. Schneidewind, A. A. Nugroho, A. Rosch, D. I. Khomskii, M. Braden, *Phys. Rev. Lett.* **123**, 017202 (2019).
 - ¹⁵ S. Kunkemöller, D. Brünig, A. Stunault, A. A. Nugroho, T. Lorenz, and M. Braden, *Phys. Rev. B* **96**, 220406 (2017).
 - ¹⁶ M. C. Langner, C. L. S. Kantner, Y. H. Chu, L. M. Martin, P. Yu, J. Seidel, R. Ramesh, and J. Orenstein, *Phys. Rev. Lett.* **102**, 177601 (2009).
 - ¹⁷ A. Kanbayasi, *Journal of the physical society of japan* **41**, 1876 (1976).
 - ¹⁸ G. Cao, S. McCall, M. Shepard, J. E. Crow, and R. P. Guertin, *Phys. Rev. B* **56**, 2916 (1997).
 - ¹⁹ S. Kunkemöller, F. Sauer, A. A. Nugroho, and M. Braden, *Crystal Research and Technology* **51**, 299 (2016).
 - ²⁰ C. W. Jones, P. D. Battle, P. Lightfoot, and W. T. A. Harrison, *Acta Crystallographica Section C* **45**, 365 (1989).
 - ²¹ B. Chakoumakos, S. Nagler, S. Mixture, and H. Christen, *Physica B* **241-243**, 358 (1998).
 - ²² S. Lee, J. R. Zhang, S. Torii, S. Choi, D.-Y. Cho, T. Kamiyama, J. Yu, K. A. McEwen, and J.-G. Park,

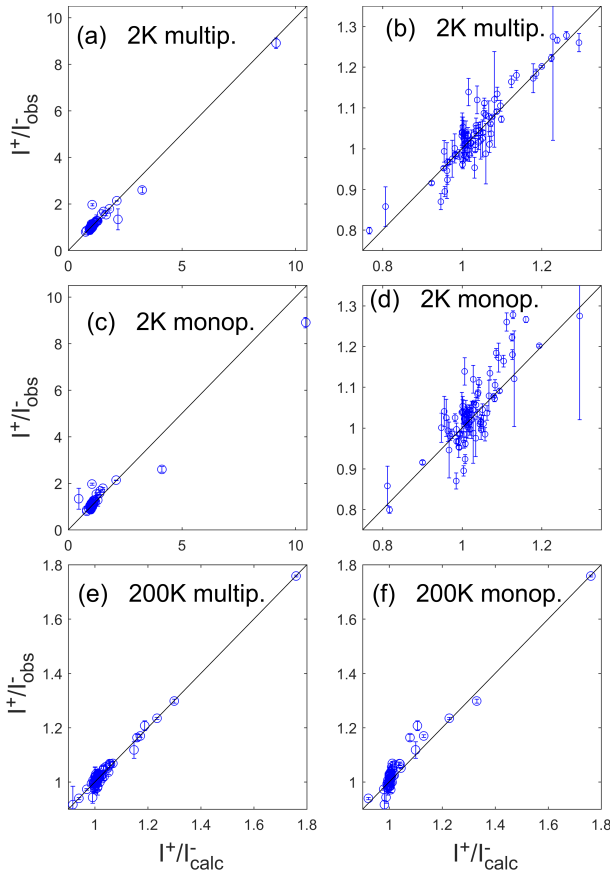


FIG. 6. Comparison of observed and calculated flipping ratios for the refinements with multipole and monopole models. For the 92(65) Bragg reflections studied at the temperature of 2(200) K the observed flipping ratios and their statistical errors are plotted against the calculated ones: in (a) and (b) the results for the multipole refinement with the 2 K data are shown; in (c) and (d) the monopole values for the 2 K dataset; in (e) and (f) the refinement results for the 200 K data are shown for the multipole and monopole model, respectively.

- Journal of Physics: Condensed Matter **25**, 465601 (2013).
- ²³ S. Bushmeleva, V. Pomjakushin, E. Pomjakushina, D. Sheptyakov, and A. Balagurov, Journal of Magnetism and Magnetic Materials **305**, 491 (2006).
- ²⁴ R. Palai, H. Huhtinen, J. F. Scott, and R. S. Katiyar, Phys. Rev. B **79**, 104413 (2009).
- ²⁵ C. Sow, D. Samal, P. S. A. Kumar, A. K. Bera, and S. M. Yusuf, Phys. Rev. B **85**, 224426 (2012).
- ²⁶ C. Etz, I. V. Maznichenko, D. Böttcher, J. Henk, A. N. Yaresko, W. Hergert, I. I. Mazin, I. Mertig, and A. Ernst, Phys. Rev. B **86**, 064441 (2012).

- ²⁷ G. Zhang and E. Pavarini, Phys. Rev. B **95**, 075145 (2017).
- ²⁸ D. C. Worledge and T. H. Geballe, Phys. Rev. Lett. **85**, 5182 (2000).
- ²⁹ S. Agrestini, Z. Hu, C.-Y. Kuo, M. W. Haverkort, K.-T. Ko, N. Hollmann, Q. Liu, E. Pellegrin, M. Valvidares, J. Herrero-Martin, P. Gargiani, P. Gegenwart, M. Schneider, S. Esser, A. Tanaka, A. C. Komarek, and L. H. Tjeng, Phys. Rev. B **91**, 075127 (2015).
- ³⁰ J. Okamoto, T. Okane, Y. Saitoh, K. Terai, S.-I. Fujimori, Y. Muramatsu, K. Yoshii, K. Mamiya, T. Koide, A. Fujimori, Z. Fang, Y. Takeda, and M. Takano, Phys. Rev. B **76**, 184441 (2007).
- ³¹ G. Baskaran, Physica B: Condensed Matter **223**, 490 (1996).
- ³² T. Rice and M. Sigrist, J. Phys.: Cond. Matter **7**, L643 (1995).
- ³³ P. Steffens, Y. Sidis, J. Kulda, Z. Q. Mao, Y. Maeno, I. I. Mazin, and M. Braden, Phys. Rev. Lett. **122**, 047004 (2019).
- ³⁴ T. Moriya, Spin Fluctuations in Itinerant Electron Magnetism, Springer-Verlag Berlin Heidelberg (1985).
- ³⁵ I. I. Mazin and D. J. Singh, Phys. Rev. B **56**, 2556 (1997).
- ³⁶ I. Eremin, D. Manske, S. G. Ovchinnikov, and J. F. Annett, Ann. Phys. **13**, 149 (2004).
- ³⁷ I. I. Mazin and D. J. Singh, Phys. Rev. Lett. **82**, 4324 (1999).
- ³⁸ A. Gukasov, M. Braden, R. J. Papoular, S. Nakatsuji, and Y. Maeno, Phys. Rev. Lett. **89**, 087202 (2002).
- ³⁹ V. Granata, L. Capogna, F. Forte, M.-B. Lepetit, R. Fitipaldi, A. Stunault, M. Cuoco, and A. Vecchione, Phys. Rev. B **93**, 115128 (2016).
- ⁴⁰ <https://www.mlz-garching.de/kompass>
- ⁴¹ S. Kunkemöller, M. Braden and A. Stunault; Institut Laue-Langevin (ILL) doi:10.5291/ILL-Data.5-51-519 .
- ⁴² J. Schweizer, in Neutron Scattering from Magnetic Materials, Editor T. Chatterji, Elsevier Amsterdam (2006).
- ⁴³ J. Rodríguez-Carvajal, Physica B: Condensed Matter **192**, 55 (1993).
- ⁴⁴ C. Frontera and J. Rodríguez-Carvajal, Physica B: Condensed Matter **335**, 219 (2003), proceedings of the Fourth International Workshop on Polarised Neutrons for Condensed Matter Investigations.
- ⁴⁵ S. F. Gull and J. Skilling, MEMSYS III Quantified Maximum Entropy Subroutine Library, Meldreth UK (1989).
- ⁴⁶ In the Fullprof suite the density maps are calculated by generating a large set of structure factors from the multipole model and Fourier transforming these.
- ⁴⁷ S. Kunkemöller, E. Komleva, S. V. Streltsov, S. Hoffmann, D. I. Khomskii, P. Steffens, Y. Sidis, K. Schmalzl, and M. Braden, Phys. Rev. B **95**, 214408 (2017).
- ⁴⁸ J. P. Perdew, K. Burke, and M. Ernzerhof, Phys. Rev. Lett. **77**, 3865 (1996).
- ⁴⁹ G. Kresse and J. Furthmüller, Phys. Rev. B **54**, 11169 (1996).